Tailored mesoporous biochar sorbents from pinecone biomass for the adsorption of natural organic matter from lake water

Tailored mesoporous biochar sorbents from pinecone biomass for the adsorption of natural organic matter from lake water

Maryam Roza Yazdani[1*], Nicola Duimovich[2], Alberto Tiraferri[2], Panu Laurell[3], Maryam Borghei[4], Julie B. Zimmerman[5,6], Riku Vahala[3]

[1] *Thermodynamics and Combustion Technology Research Group, Department of Mechanical Engineering, School of Engineering, Aalto University, P.O. Box 14400, FI-00076 AALTO, Finland*

[2]*Department of Environment, Land and Infrastructure Engineering (DIATI), Politecnico di Torino, Corso Duca degli Abruzzi 24, 10129, Turin, Italy*

[3]*Water and Environmental Engineering Research Group, Department of Built Environment, School of Engineering, Aalto University, P.O. Box 15200, FI-00076 AALTO, Finland*

[4]*Molecular Engineering of Bio-synthetic Materials Research Group, Department of Bio-products and Bio-systems, School of Chemical Engineering, Aalto University, P.O. Box 16300, FI-00076 AALTO, Finland*

[5]*Chemical and Environmental Engineering, Yale University, 17 Hillhouse Avenue, New Haven, Connecticut 06511, United States*

[6]*School of Forestry and Environmental Studies, Yale University, 195 Prospect Street, New Haven, Connecticut 06511, United States*

*Corresponding author`s email: roza.yazdani@aalto.fi; rozmaryam.yazdani@gmail.com

Abstract

Natural organic matter (NOM) raises major issues for drinking water treatment including undesirable taste and color, formation of carcinogenic disinfection by-products (DBPs), and promotion of microbial regrowth in the water distribution system. As such, mesoporous biochars have been tailored from pine-forestry by-products for treating NOM and color causing compounds from drinking water sources, such as lakes. Herein, several tailored biochars are fabricated via two procedures: pre-pyrolysis/activation/post-pyrolysis and activation/post-pyrolysis processes, using NaOH and $ZnCl_2$ activators to improve the surface chemistry and porous structure for higher NOM adsorption. The mesoporous biochars, pristine biochars, and pinecone biomass are characterized via several characterization analyses including Brunauer, Emmett and Teller surface area measurement (BET), thermogravimetric analysis (TGA), and scanning electron microscopy (SEM). Batch experiments are conducted to study the adsorption isotherm, kinetics and mechanism along with desorption. Characterization revealed effective characteristics of tailored biochars for NOM adsorption including mesoporous structure, remarkable surface area (up to 1470 m^2/g), high thermal stability, and elevated carbon content. All the tailored biochars showed improved removal capacities for NOM and color compounds from real lake water samples compared with those of the pinecone biomass and pristine biochars. The most promising tailored biochar (herein named as TB-N-I) was developed by NaOH modification via pre- and post-pyrolysis processes. With the lowest optimized dosage (0.25 g/L), TB-N-I removed more than 80 % of both NOM and color from the lake water (COD: 13.4 and color: 53.65 mg/L), superior to the removal capacity of commercial powdered activated carbon (PAC). Acidic conditions significantly favored the adsorption, e.g., NOM removal by TB-N-I from the lake water reached 97 % at pH 2. Nonlinear regression provided a good fit for Freundlich and Sips (r^2= 0.988 and Δq=0.08) isotherms as well as pseudo-second-order kinetic models. This suggests the heterogeneous distribution of the adsorptive sites at the biochar surface and the multilayer nature of NOM adsorption. A desorption study revealed that more alkaline solutions resulted in higher NOM desorption (30 mM NaOH > 3 mM NaOH > distilled water), yielding regenerated adsorbents with high re-adsorption capacity. Liquid chromatograph–organic carbon detection (LC-OCD) was used to study the removal of different NOM size fractions, e.g., low molar mass (LMM) fraction of NOM, which are more hydrophilic and resistant to conventional treatments. Of significant interest, LC-OCD indicated that TB-N-I removed 20% more of the problematic LMM compared with that of PAC. Effective pore size distribution of tailored biochar (TB-N-I) for the adsorption of NOM fractions was indicated by BET analysis and was confirmed by LC-OCD.

Keywords: Biochars; Modification; Mesoporosity; Adsorption; Natural organic matter; Removal mechanism

1. Introduction

Biochars are being utilized for a wide range of applications, including environmental management such as remediation of soil, management of waste, and mitigation of climate change [1-3]. Thermal treatment of biomass via pyrolysis in a limited oxygen atmosphere results in biochar, bio-oil, and syngas [3, 4]. Biochar production from waste biomass is both economical and environmentally beneficial [1]. Owing to their porous structure, relatively high surface area, and enriched surface chemistry, there is a growing interest for biochars as sustainable media in engineering value-added materials [2]. They can be produced near the point of application and/or near biomass sources in both small-scale pyrolysis units and in large-scale integrated refinery facilities that are designed for simultaneous biochar and energy production.

The biomass composition and production conditions can influence the yield and properties of the biochars [5]. Biochars are typically developed from abundant biomass sources such as wood. Low-temperature pyrolysis (400-500 °C) yields enriched porous biochars with low oxygen and hydrogen content [4]. Biochars developed at higher temperatures (>700 °C) provide elevated aromaticity, hydrophobicity, surface area, mesopores and micropores. These properties make them a high quality and eco-friendly alternative to, for instance, coal-based activated carbons for water purification [6]. Surface properties of biochars can be also manipulated through activation/modification [7]. Chemical activation uses chemicals to oxidize the surface and generate desired functional groups [7]. Enhanced oxygen-containing surface functional groups enable the possibility of specific binding (e.g., hydrogen bonding and π-π electron-donor–acceptor interactions) [8]. The hydrophobic surface of biochars results in adsorption affinity for hydrophobic organic compounds, including pharmaceuticals and natural organic matter (NOM) [4, 6].

Agricultural and forestry by-products such as pinecones can be tailored into value-added materials, such as biochars, providing adsorptive properties for contamination remedies [5, 6, 8-15]. The pine family comprise economically important species in agriculture and forestry industries worldwide, especially in the Nordic countries. These species produce large quantities of pinecones as by-products annually. Pinecones are composed of imbricated woody scales, containing cellulose, hemicelluloses, and lignin. Availability and high lignocellulosic content make pinecone a suitable and cost-effective biomass for biochar production. Unmodified biochars however exhibit limited adsorption for anionic species [12]. The biochars can be further modified through chemical or physical processes to increase their adsorptive properties according to the target pollutant, the environmental condition, and the treatment goals [16]. Herein, we aim to tailor mesoporous biochars through chemical modification for the adsorption of NOM from lake water. Tailoring through chemical modification, e.g., alkali activation, can enhance the surface functionality and structure of biochars [7] for higher adsorption of our target pollutant, NOM, from lake water.

NOM in natural water sources negatively affects the drinking water treatment and the finished water quality. For instance, it causes taste and color problems, raises the coagulant and oxidant/disinfectant demand, acts as a precursor to disinfection by-products (DBPs), and promotes microbial regrowth in water distribution system [17, 18]. NOM is treated conventionally by chemical coagulation, or by adsorption onto activated carbon (AC) [19]. The adsorption depends on the characteristics of the NOM, the adsorbent and the water. For instance, molecular mass size and hydrophobicity of NOM control its adsorption. NOM consists of high molar mass (HMM) fraction such as humic compounds, easily removable by coagulation, and intermediate molar mass (IMM) compounds, more controllable by adsorption [17, 19]. However, of significant concern is the low molar mass (LMM) fraction of NOM such as tannic acids, which are more hydrophilic and resistant to common treatments. As NOM adsorption primarily takes place by pore filling mechanism, it is largely influenced by the relationship between the pore size distribution of the adsorbent and molecular size of NOM [17]. Mesopores (2-50 nm width) accompanied with sufficient amount of micropores (< 1 nm in width) can therefore provide high adsorption capacities for different fractions of NOM e.g. LMM [17, 19].

Our objective is to tailor biochars with high content of mesopores accompanied with microspores and desired surface functional groups though chemical modification towards higher adsorption of NOM, especially the problematic LMM fraction, from lake water. The adsorbents are fabricated via two pathways involving one-step pyrolysis or two-step pyrolysis. Sodium hydroxide, NaOH, and zinc chloride, $ZnCl_2$, are used to modify the interfacial and structural properties of the pinecone-derived biochar for higher adsorption of NOM. However, adsorption studies are mainly performed under single-solute condition (synthetically made organic matter solutions) and are not evaluated for the treatment of natural water, e.g. lake water. It is important to scrutinize the removal performance of the developed adsorbents in representative water matrices as was done in this study. To study their structure and composition, the adsorbents are characterized via characterization methods such as Brunauer, Emmett and Teller (BET) specific surface area/porosity, thermogravimetric (TGA), and scanning electron microscopy (SEM). The tailored biochars are evaluated for removing NOM and color causing compounds from lake water through adsorption equilibrium, kinetics, and mechanism and are compared with a commercial coal-based powdered activated carbon (PAC). The adsorption of different NOM fractions, such as humic substances and LMM acids, by mesoporous biochars and PAC are also analyzed via liquid chromatograph–organic carbon detection (LC-OCD).

2. Methodology

2.1. Materials

Pinecone biomass was obtained from Otaniemi campus of Aalto University, Finland, between September and November. The cones were washed repeatedly with tap and reverse osmosis water to remove impurities,

dried at 80°C for 24 h and crushed. The dried biomass was ground in a blender (11 basic Analytical mill, IKA) and sieved using 80-µm sieve (Retsch GmbH Germany). The powdered biomass was stored at room temperature in the dark and used for tailoring biochars. NaOH and $ZnCl_2$ were purchased from Sigma Aldrich. A commercial coal-based powdered activated carbon (PAC) (Merck) was used for comparison. Sulphuric acid, potassium permanganate, potassium iodine, starch-indicator, and sodium thiosulfate (Sigma Aldrich) were used for the determination of chemical oxygen demand calibration curve.

2.2. Fabrication of mesoporous biochars

Four types of biochars were tailored via one-step and two-step pyrolysis involving chemical modification; see the illustration of the fabrication pathways as Figure 1 in [20]. In the pre-pyrolysis/activation/post-pyrolysis process (I), dried powdered biomass was first pyrolyzed at 300 °C for 15 min under nitrogen gas (1 L/min) in a laboratory-scale batch tube furnace (NBD-O1200, Nobody Material Science and Technology CO., LTD, China). The weight loss from the thermal treatment was measured; 66±1% yield was achieved. Secondly, the biochars were modified with NaOH and $ZnCl_2$. Pristine biochars were mixed with chemical solutions (1/2 weight ratio of biochar/activator) for 2 h, dried overnight at 105 °C, and thirdly heated for 2 h under nitrogen gas at 800 °C. In the activation/post-pyrolysis process (II), dried powdered biomass was first mixed with the chemical solutions (1/2 weight ratio of biomass/ activator) for 30 min followed by heating in an oven at 105 °C for 24 h. After drying, it was pyrolyzed at 700 °C for 2 h under nitrogen gas (1 L/min). The products were rinsed with 0.1 M HCl and reverse osmosis water until neutral pH was reached and dried at 105 °C for 24 h. The dried biochars were finally ground, sieved using 80 µm sieve, and stored at room temperature in the dark for characterization and adsorption. The samples are referred to as tailored biochar (TB)-activator (NaOH: N or $ZnCl_2$: Z)-method (II or I) e.g., TB-N-I. For comparison, pristine biochars were also produced via pyrolysis at 300 and 700 °C (referred as B-300 and B-700).

2.3. Characterization of mesoporous biochars

Brunauer, Emmett and Teller (BET) specific surface area and porosity analysis was conducted using Tristar II-Micromeritics, USA, via the adsorption-desorption cycle of N_2 gas at 77.350 K onto the external surface of

the materials. Scanning electron microscopy (SEM) was carried out on a ZEISS SIGMA VP (1.8-2.0 kV acceleration voltage) to explore the surface morphology. Energy dispersive X-ray (EDX) analysis was performed on a JEOL JSM-7500FA analytical field Emission scanning electron microscope (15 kV acceleration voltage, emission current of 10 µA). To study the thermal stability, we carried out thermogravimetric analyses (TGA) on TA instruments – TGA Q500 (USA) from 20 °C to 800 °C at a heating rate of 10 °C/min under N_2 gas environment. A Nicolet 380 FT-IR infrared spectrometer was used for Fourier transform infrared spectroscopy (FTIR).

2.4. Raw water samples

Lake water samples were collected from Lake Pitkäjärvi in Espoo, Finland. Table 1 compiles the quality characteristic of the lake water.

Table 1

2.4.1. NOM and color measurement

The concentration of NOM was estimated via UV absorbance measurement at 254 nm wavelength, using a UV-1201 Shimadzu-spectrophotometer. The samples were filtered before the measurement through Sartorius Minisart 0.45 µm filters. The absorbance was converted to concentration using the COD_{Mn} calibration curve, see Figure 2 in [20]. To measure COD_{Mn}, a known amount of potassium permanganate ($Na_2Sa_2O_3$) was added to acidified lake water samples using 4 M sulfuric acid. The samples were boiled for 20 minutes, where the oxidizing matter in the samples reduces part of the permanganate. The unreduced portion of permanganate was measured by iodometric titration method and the amount of used permanganate was used to calculate COD_{Mn}. The color of water samples was measured according to the SFS-EN ISO 7887. Samples were filtered and the absorbance was measured at 410 nm wavelength.

2.4.2. Liquid chromatograph – organic carbon detection (LC-OCD) measurement

Liquid chromatograph–organic carbon detection (LC-OCD) quantifies the elution as a function of size and affinity of carbon from a Toyoperal HW 50 s column using a buffered carrier solution [21]. The method was

calibrated using Suwannee River humic and fulvic acid standards. UV254 absorbance and organic carbon were measured online and allowed quantifying the elution of DOC over time. UV254 absorbance was measured with a K200 detector by Knauer, organic carbon was measured by first decomposing it to carbon dioxide (CO_2) in a Gräntzel-reactor and then measuring the CO_2 with Ultramat 6 infrared detector by Siemens. FIFFIKUS software was used to separate the acquired chromatograph into different apparent size fractions, viz. biopolymers (molecular weight (MW) > 20 kDa), humic substances (MW ~ 1000 Da), building blocks (MW 300-500 Da), low molecular weight acids (MW < 350 Da), and low molecular weight neutrals (MW < 350 Da).

2.5. Adsorption

Known amount of the adsorbent in 50 mL volume of lake water were used for the adsorption batch experiments on a shaker (150 rpm and room temperature). The experiments were carried out without pH adjustment, except for those studies where indicated. After the desired contact time, the solutions were filtrated through Sartorius Minisart 0.45µm filters for the final COD_{Mn} concentration measurement. The adsorbent dosage was optimized within 0.1–1 g/L range. The effect of pH was investigated through adjusting the solution pH at values 2, 4, 8, and 10 using HCl and NaOH. The kinetics were explored at varying time intervals between 1 min to 24 h. The batch experiments were conducted in two or three replicates. We employed the following equations to determine the removal percentage and adsorption capacity:

$$\text{Removal } \% = \frac{(C_i - C_t)}{C_i} \times 100 \quad (1)$$

$$q_t\ (\text{mg/g}) = \frac{C_i - C_t}{m} \times V \quad (2)$$

where C_i and C_t (mg/L) are the initial COD_{Mn} concentration and the concentration at time t, respectively, V (L) is solution volume, and m (g) is adsorbent mass.

2.6. Desorption and re-adsorption

For desorption and re-absorption batches, 0.25 g/L dosage of TB-N-I was used to treat the lake water without pH adjustment. After first adsorption, the spent adsorbent was collected via vacuum filtration and dried overnight at 40 °C. The kinetics of desorption was studied with three desorption solutions, deionized water,

3 mM NaOH, and 30 mM NaOH at several time intervals between 1 min to 24 h. The batch tests were conducted on a shaker at 150 rpm and at room temperature, using 50 mL desorption solution and 0.25 g/L spent adsorbent. After desorption, the adsorbent was collected and dried at 40 °C overnight to be used for re-adsorption in a similar condition as the first adsorption. Desorption is determined as follows:

$$\text{Desorption } \% = \frac{C_{des}}{C_i - C_{ads}} \times 100 \quad (3)$$

where C_{ads} is the COD_{Mn} after first adsorption, and C_{des} is the COD_{Mn} after desorption.

2.7. Theoretical analyses

The isotherms and kinetics of adsorption were analyzed via non-linear regression. We used Langmuir [22], Freundlich [23], and Sips [24] isotherm models and Lagergren's pseudo-first order [25] and pseudo-second order [26] kinetic models (see Table 1 in [20] for the equations). Weber and Morris intra-particle diffusion model [27] was used to explore the diffusion mechanisms involved in NOM adsorption (see Table 1 in [20]). The coefficient of determination, r^2, and normalized standard deviation, Δq, (see Table 1 in [20]) were used to find the best-fitting nonlinear model and to quantitatively compare the applicability of the models.

3. Results and discussion

3.1. Characteristics of the adsorbents

3.1.1. Infrared spectroscopy

The FT-IR spectra of the initial and tailored materials are given Figure 1a. The spectra of the pinecone and the pristine biochar showed several significant bands. The bands at 3400-3300 cm^{-1} correspond to O-H stretching, at 2920 cm^{-1} and 2870 cm^{-1} indicate asymmetric and symmetric C-H, at 1600 cm^{-1} are related to C=C stretching, at 1240 cm^{-1} are for C-O stretching, and at 1010 cm^{-1} indicate C-H out-of-plane bending (e.g. aromatic structure of lignin) [15, 28]. No characteristic band was observed for the TBs, confirming the gasification and conversion to graphitic structure. For instance, the disappearance of O-H stretching vibration bands for all the tailored materials suggests the oxygen in the initial materials was removed during fabrication and phenolic-aromatic structures were cracked to leave carbon solids [28]. Similar results have been reported on pinewood biochar [15].

Figure 1

3.1.2. Thermogravimetric and elemental analyses

The mass variation of the adsorbent materials as a function of temperature (TGA) is shown in Figure 1b. TGA confirmed a high thermal stability of the tailored biochars. Three stages can be distinguished during the pyrolysis of lignocellulosic materials, also observed for the pinecone biomass in Figure 3a in the reference [20]. They include (I) dehydration below 150 °C, (II) primary pyrolysis between 200 to 480 °C with evolution of most gases and tars and the formation of the basic structure via decomposition of hemicellulose and cellulose, and (III) consolidation of the biochar structure at 500-800 °C with a small weight loss via devolatilization of residual char and lignin [5, 29]. The pristine biochar also went through a large mass loss between 300 °C and 500 °C. Compared with the biomass and pristine biochar, the tailored biochar showed high thermal stability. The elemental analysis of the tailored biochar (TB-N-I) (see Figure 3c in [20]) confirmed that TB-N-I consists mainly of carbon (84 wt. %) and other elements including oxygen (1.6 wt. %) and nitrogen (12.7 wt. %) in minor contents.

3.1.3. Surface area and pore size distribution

Specific surface area and porosity are among the key properties of adsorptive materials. Table 2 compiles the BET surface area, pore volume, and pore size of the initial and tailored materials. The biomass and pristine biochar (B-300) have low specific surface areas, 0.491 m^2/g and 0.583 m^2/g, and pore volume, 0.001 and 0.001 cm^3/g, respectively. This may be due to the presence of hemicellulose, cellulose, and lignin in the tight structure of the initial materials. Since B-300 was pyrolyzed at relatively low temperature (300 °C), the lignocellulosic framework was partially degraded resulting negligible increase in surface area and pore volume. The biochars tailored through both fabrication pathways, TB-N-I and TB-Z-II, showed remarkable increase in specific surface area, 1470.3 and 1067.9 m^2/g, and pore volume, 0.705 and 0.511 cm^3/g, which were higher than those of commercial PAC, 819.475 m^2/g and 0.325 cm^3/g, respectively. Chemical activation enhances pore development and builds new pores, with elevated BET surface area upon increasing the post-pyrolysis temperature [9].

Table 2

The nitrogen gas adsorption–desorption isotherms results are depicted in Figure 1c. The shape of adsorption isotherm discloses qualitative information about the adsorption mechanism and the pore structure of the materials [10]. Adsorption isotherms of the biomass and pristine biochar show characteristics of type II isotherm, indicating adsorption onto macroporous materials with strong adsorbate-adsorbent interactions. Further, the isotherm curves remained unclosed at lower relative pressure region (see Figure 3b in [20]), resulted from capillary condensation phenomenon. Chemisorption at a certain number of pores with strong chemical potential may prevent desorption of the adsorbed nitrogen at low pressure [10]. The shape of the N_2 adsorption-desorption isotherms along with low surface area and pore volume indicates that the biomass and the pristine biochar provide limited pores. The isotherms of TBs show a predominantly mesoporous structure of the developed carbons, resulting in a gradual increase in adsorption after the initial filling of the micropores, followed by an enhancement near saturation. They can be classified as a combination of type I and type IV isotherms with hysteresis loops appeared at higher relative pressure region, indicating the wide mesopore distribution in the materials [10, 13]. The development of highly mesoporous structure along with some degree of micropores for the tailored biochars is further confirmed by the pore size distributions shown in Figure 1d.

Figure 1

The pore size distribution of the tailored biochars mainly ranged within 2 nm to 10 nm, with the average pore diameters of 2.96 and 2.68 nm for TB-N-I and TB-Z-II, respectively, confirming mesoporous characteristics (Table 2). The porous materials can include three categories of micropores (< 2 nm), mesopores (2-50 nm) and macropores (> 50 nm). Both micro-pores and meso-pores contents are enhanced in the modified biochars compared to those of the biomass and the pristine biochar. The tailored biochars contain both mesopores and micropores, yet the volume of mesopores was larger than that of micropores. The TBs benefit from the mesoporous structure with higher surface area and narrower pore size distribution, providing high accessibility for higher molecular weight NOM fraction and wider transport channels to micropores for the

lower molecular weight components of NOM (LMM). The mesoporous structure of the TBs is confirmed by SEM images in Figure 1e, which show the presence of microspores and mesopores. Table 3 compares the characteristics of biochars developed from forestry and agricultural wastes for pollutant removal.

Table 3

3.2. Adsorption of NOM and color from lake water

3.2.1. Dosage of adsorptive materials

Figure 2 shows NOM and color removal upon dosing of the adsorbents. The biomass and two pristine biochars were unsuccessful in removing both NOM and color from the lake water samples (removal percentage < 25 %). A remarkable improvement was observed in the adsorption of NOM and color by all tailored biochars: the removal increased with dosage. TB-N-I exhibited almost 300 % improvement in NOM adsorption from lake water compared with those of the biomass and pristine biochars. An increase from 0.2 to 1 g/L of TB-N-I dosage improved the NOM removal from 76 % to 87 % and the color removal from 77 % to 93 %, respectively. Alkali activated biochars generally provided higher efficiency for removing target contaminants from the lake water. Compared with PAC, TB-N-I performed noticeably better, in lower doses e.g. 0.2 g/L TB-N-I removed 76% NOM compared with 60 % removal by 0.2 g/L PCA. The adsorption of NOM molecules primarily occurs via physisorption e.g., pore filling and hydrophobic attraction through π-π electron donor-acceptor [1], which are promoted by improved surface and pore characteristics of our tailored biochars (Table 2). Higher NOM removal yields from both higher surface area and mesoporosity and the larger amount of hydroxyl groups generated by alkali activation [7].

Figure 2

TB-N-I provided the highest adsorption percentage (80 %) and capacity (36 mg/g) with the lowest optimized dose (0.25 g/L) that were superior to those obtained by PAC (75%; 27 mg/g; 0.3 g/L). The optimized adsorbent dosage is illustrated in Figure 4a in reference [20]. Furthermore, Figure 2c shows the effect of concentration (dilutions of lake water) on NOM removal by 0.25 g/L TB-N-I at three contact times, viz. 0.5 min, 30 min, and 1440 min. The TB-N-I was able to effectively remove NOM from lake water across NOM concentrations. For

instance, after 1440 min of contact time, 72 % (9.97 mg/g) and 83 % (2.63 mg/g) of NOM were removed from 10 and 2.5 mg/L initial concentrations, respectively.

3.2.2. Water pH

The characteristics of the pollutant, the adsorbent and the water matrix define the interface chemistry [30-32]. The pore size distribution plays a key role in NOM uptake, yet electrostatic attraction serves as the secondary controlling factor [17]. NOM and color adsorption from the lake water were examined by varying pH in the 2-10 range. As shown in Figure 3, the removal of both NOM and color by the engineered adsorbents generally increased upon decreasing pH. The highest removal was achieved by TB-N-I with 97% NOM and 97% color removal at pH 2 while these amounts deceased to 73% NOM and 70% color removal at pH 10. A lower pH-dependency was observed for the adsorption of NOM onto TB-N-I compared with that of PAC. A higher pH-sensitivity was observed for the color adsorption compared with NOM adsorption, which can be an indicative for the ionic nature of color causing compounds in lake water (Figure 3). These are promising results in practical perspective, indicating the potential of our tailored biochars for effective NOM removal in a wide range of pH (with or without pH adjustment).

Figure 3

The solution pH regulates the protonation and deprotonation of both NOM fractions and biochars. While at lower pH, the attraction between protonated surface and the dissociated carboxylic group ($pK_a \sim 3$) accounts for the adsorption of humic substances, at relatively higher pH the interaction between adsorbent and neutral phenolic group ($pK_a \sim 9$) dominates [33]. The surface of the tailored biochars shows an amphoteric character. The point of zero charge (pH_{PZC}) for activated carbons and biochars has been reported around 7 to 8.5 [34, 35], which is consistent with the pH shift observed during our pH study (see Figure 4b in [20]). The surface is positively charged at pH 2, partly due to the donor/acceptor interactions between the char structure and the hydronium ions [35]. As there is a lower repulsion between NOM molecules adsorbed on the surface and in the solution, the humic substances can pack closely on the surface. A declining adsorption upon increasing pH suggests the electrostatic attraction being superior to the hydrogen bonding mechanism

[35]. Herein, the decreasing adsorption from pH 2 to 6 is caused by the progressively deprotonated surface towards becoming uncharged, lowering the electrostatic interactions. As pH increases from 6 to 10 (Figure 3), the surface protonation is reduced and the hydrogen bonding become gradually dominant. Furthermore, because of their relatively low charged character and physical intermolecular interactions e.g., Van der Waals forces, humic substances aggregates at lower pH values, yielding a higher thickness and adsorbed NOM mass. By raising pH, the charge density on the humic macromolecules increases due to the ionization of their acidic groups, which leads to intra- and intermolecular electrostatic repulsion. Consequently, the NOM macromolecules gradually become non-aggregated, causing a thinner NOM layer thickness and lower adsorbed mass [36].

3.2.3. Kinetics

Figure 4 shows NOM and color removal by the TBs at different time intervals. The adsorption proceeds in two stages: a rapid uptake of the molecules within first 60 min, with 74.3 % and 59 % NOM removals by TB-N-I and PAC, respectively. A slower stage appears afterwards until the equilibrium is reached within 360 min, corresponding to 80.8 % removal by TB-N-I and 71.2 % removal by PAC. Similarly, color removal increased with contact time with the TBs.

Figure 4

When comparing the pseudo kinetic models, the experimental kinetic data showed a better fit to pseudo-second-order model (according to r^2 and Δq values in Table 4). In nonlinear regression, a high value for the determination coefficient (r^2) together with a small value for normalized standard deviation (Δq) suggest good fitting of a model to experimental data [30, 37]. For all our studied cases, pseudo-second-order provided higher r^2 values and smaller Δq values (e.g. r^2= 0.814 and Δq=0.124 for TB-N-I) compared with those of pseudo-first-order model (e.g., r^2= 0.667 and Δq=0.161 for TB-N-I).

The diffusion mechanisms of adsorption were studied by intra-particle diffusion model. As depicted in Figure 5a, the graphs of q_t versus $t^{1/2}$ are multi-linear including at least two linear stages. Adsorption proceeds in four consecutive steps [38] including film diffusion through the boundary layer to the external surface and the intraparticle diffusion (pore and surface diffusions) into the interior of the adsorbent. The total rate of

adsorption is generally determined by film and/or intraparticle diffusions. The molecule transfer within the interior of the adsorbent normally occurs by pore and surface diffusions, yet their magnitudes are hardly determined. Thus, only a general intraparticle diffusion mechanism is assumed as predominant [38]. The multi-linearity of Figure 5a and C values in Table 4 suggest that the intraparticle diffusion is one of the stages involved in the NOM adsorption [30]. Film diffusion is the rate controlling stage in the initial NOM adsorption onto the exterior surface, afterwards proceeding by intra-particle diffusion into the pores.

Table 4

3.2.4. Isotherm

Adsorption isotherms determine the distribution of NOM molecules between the surface and solution at equilibrium. NOM adsorption isotherms are shown in Figure 5b. The adsorption increases sharply with increasing NOM equilibrium concentration, which is indicative of numerous readily accessible adsorption sites. Moreover, higher NOM adsorption is observed for TB-N-I compared with that of PAC.

Figure 5

The equilibrium data are modeled by nonlinear Langmuir, Freundlich, and Sips isotherms. Freundlich and Sips isotherms described the adsorption equilibrium data slightly better in terms of giving higher values for r^2 and lower values for Δq (Table 5). This suggests the heterogeneous distribution of the available active sites at the solid surface and the multilayer nature of adsorption. The Sips isotherm relates systems where one adsorbed molecule can get involved with more than one adsorptive site [30, 37].

Table 5

3.2.5. Removal mechanism

Characterization of NOM gives important information on the quality of the raw and treated water along with the process performance. NOM in water can be characterized by e.g., degree of aromaticity, amino acid content, and molar mass [18]. NOM fractions in both lake water and treated water samples were characterized by LC-OCD analysis and the results are given in Table 6 and Figure 6.

Table 6

LC-OCD detected different NOM fractions, such as HMM humic substances and LMM organic acids. LC-OCD results in Table 6 show that both TB-N-I and PAC, have effectively removed humic substances (HS) and building blocks: 74.0% and 74.0% removals for TB-N-I and 59.8% and 68.9% for PAC, respectively. Biopolymers were not retained as well; PAC was able to remove only 24.3 % while TB-N-I retained 61.1%. As NOM adsorption primarily takes place in mesopores and large micropores (1-2 nm width) [39, 40], these results again suggest that TB-N-I has better range in pore size (consistent with the BET results in Table 2). DOC uptake from lake water (Table 1) for PAC was approximately 81% of that obtained by TB-N-I. Table 6 also presents the average molar mass (MM) of HS, which increases from raw water sample to water samples treated by PAC and TB-N-I, respectively. Accretion in average MM indicates that IMM and LMM compounds are removed more effectively than HMM compounds. Consequently, TB-N-I is more efficient in removing small size HS compared with PAC. These results confirm that the adsorbability of NOM increases with decreasing molecular size, as suggested by Velten et al. [17] (i.e. biopolymers < HS < building blocks < LMM compounds). With LMM compounds, however, there is a clear difference between LMM neutrals and LMM acids. LMM neutrals, which are weakly or uncharged hydrophilic or slightly hydrophobic ("amphiphilic") compounds, are retained well by both adsorbents (77.7% and 58.3% for TB-N-I and PAC, respectively). On the other hand, the concentration of LMM acids, fraction containing all aliphatic organic acids, increases with both PAC and TB-N-I treatment. As NOM with MM < 500 mg/l produces significant amount of disinfection by-products [41, 42], their efficient removal is desirable. In this study, TB-N-I has removed 20% more LMM NOM, including building blocks, LMM neutrals, and LMM acids, compared to PAC.

Figure 6

Chromatograms eluted for organic carbon (OC) and UV detection from LC-OCD analyses are shown in Figure 6 for raw and treated water samples with TB-N-I and PAC. The chromatogram for OC exhibits a peak for biopolymers followed by large peak for humic substances and building blocks of humic substances. LMM organics include both LMM acids and LMM humics, latter ones are later subtracted. Compared to the chromatogram obtained with OC detection, that obtained with UV detection shows that TB-N-I treatment

436 has retained more UV absorbing compounds than total NOM removal. Relative signal strength for raw water
437 is higher for UV compared to OC, while it is lower for PAC effluents.
438
439 The effective adsorption of NOM by our mesoporous biochars is mainly owing to the high surface area, meso-
440 porosity, and large hydroxyl group contents generated by alkali activation. Our high temperature derived
441 biochars also provide high surface aromaticity for a higher NOM sorption. Nevertheless, the nature and
442 functionality of the target organic compounds also affect their affinity for adsorption onto the TBs. The
443 mechanisms involved in NOM adsorption are explored in terms of multicomponent adsorption of its different
444 fractions. While polar fraction is removed by hydrogen bonding with the surface functional groups of the TBs,
445 non-polar fraction is attracted through hydrophobicity [1]. Furthermore, depending to the water chemistry,
446 the amphoteric surface of TBs gets positively or negatively charged causing electrostatic forces for charged
447 organic compounds. Aromatic π-systems in biochars provide high content of electron-withdrawing functional
448 groups, acting as π-acceptors for electron donors [1]. Both electron -rich and -poor functional groups are
449 present in high temperature derived biochars, enabling interactions with both electron donors and electron
450 accepters. At acidic environment, the π–π electron donor–acceptor interactions between π-electron -rich
451 surface and π-electron deficient organic compounds take place. At alkaline medium, adsorption is involved
452 with proton exchange with water and formation of hydrogen bonds between the organic compounds and a
453 surface carboxylate or phenolate, classified as a negative charge-assisted hydrogen-bond [43].
454
455 Figure 7 illustrate the dominant mechanisms contributing for the adsorption of NOM, including pore filling,
456 π–π interactions, polar/electrostatic interactions, and hydrogen-bonding [1, 44]. However, the relative
457 contribution of these mechanisms to total adsorption is under debate. The more hydrophobic humic
458 substances attach to the mostly π-rich adsorptive sites so that hydrophobic interactions, e.g. π–π
459 interactions, contribute for the higher adsorption. However, the adsorption of hydrophilic LMM, e.g. tannic
460 acid, is accompanied with their smaller molecular size and easier reach to the inner meso- and micro-pores.
461 The relatively π-poor LMM fraction contain hydrophilic functional groups, e.g., digallic acid, enabling a
462 monolayer adsorption. Contrarily, the π-rich humic macromolecules with structural benzene rings can pile

up at the preoccupied adsorptive surface with humic compounds [4]. Nevertheless, diverse polar functional groups on the structure of these compounds increase the adsorption affinity via hydrogen bonds and polar interactions with the engineered surface. Thus, there is more multi-layer adsorption onto mesoporous TB-N-I than microporous PAC. In summary, higher adsorption of NOM onto TB-N-I originates from the presence of more adsorptive sites through meso-porosity, high aromatic surface area, and alkali-generated hydroxyl groups, resulting in the higher adsorption affinity of LMM NOM than those provided by the microporous PAC.

Figure 7

3.3. Desorption–re-adsorption

To study the chemical regeneration potential, the desorption process on the spent tailored biochars was performed in three regeneration systems, e.g. distilled water, 3 mM NaOH and 30 mM NaOH (see Figure 5 in [20]). The desorbed NOM concentrations at several time intervals were determined. The desorption increased at higher alkaline medium as 30 mM NaOH > 3 mM NaOH > distilled water. It was also observed that desorption increases upon increasing time: up to 62 % desorption was achieved within 3 h, afterwards gradually raised up to 70 % within 24 h. These results indicate the adsorption of NOM onto TB-N-I is mostly reversible and the spent adsorbents show high capacity for regeneration. The second cycle of NOM adsorption on regenerated TB-N-I was performed at different time intervals. It was observed that re-adsorption increased by time (see Figure 5b in [20]). The adsorption capacity of virgin TB-N-I within 3 h of contact time was around 12.5 mg/g, while NOM adsorption on the regenerated TB-N-I amounted 13.8 mg /g. The regenerated TB-N-I possessed a high adsorption capacity and hence could be utilized repeatedly for NOM adsorption.

4. Conclusions

Natural organic matter (NOM) in drinking water treatment serves as precursors to disinfection by-products (DBPs) and promotes microbial regrowth in the water distribution system. Renewable pinecone biomass has been used to tailor mesoporous biochars for removing NOM from lake water. The adsorbents were fabricated via pre-pyrolysis/activation/post-pyrolysis and activation/post-pyrolysis processes, using chemical activators

to enhance the surface chemistry and porous structure for a higher NOM uptake. Characterization analyses e.g. BET, SEM, EDX, FTIR, and TGA revealed high thermal stability, mesoporous structure, remarkable surface area (up to 1470 m^2/g), elevated carbon content and surface functionality of the engineered products. Our tailored biochars showed superior removal capacities for NOM and color from lake water compared with those of the biomass and pristine biochars. The most promising tailored biochar (TB-N-I) was prepared via NaOH activation accompanied with pre- and post-pyrolysis. With lowest 0.25 g/L dosage, TB-N-I removed more than 80 % of both NOM and color, a superior removal capacity compared to that of commercial activated carbon (PAC). Effective NOM and color removals were achieved under a wide pH-range, e.g. TB-N-I removed 97 % of NOM at pH 2. Nonlinear regression showed good fits for Freundlich and Sips isotherm and pseudo-second-order kinetic models with the experimental data. Higher alkaline mediums (30 mM NaOH > 3 mM NaOH > distilled water) provided higher desorption resulting in regenerated adsorbents with large re-adsorption capacities. Liquid chromatograph–organic carbon detection (LC-OCD) detected different NOM fraction in the lake water and was used for enlightening the mechanisms involved in NOM adsorption. LC-OCD results suggested that TB-N-I was more effective in removing the problematic low molar mass (LMM) compounds compared to PAC. In summary, the experimental results and theoretical analyses confirm the high potential for the applicability of our tailored biochars for NOM treatment.

Acknowledgments

We conducted the experiments at *Aalto University*'s analytical water laboratory. We would like to thank *Mehrdad Hesampour*, *Kemira Oyj*, for the assistance with Liquid chromatograph – organic carbon detection (LC-OCD) and *Ari Järvinen* and *Aino Peltola*, *Aalto University*, for their help with NOM measurements. The first author gratefully acknowledges *Doctoral School of Aalto University* and *Foundation for Aalto University Science and Technology* for their financial support.

References

[1] M. Ahmad, A.U. Rajapaksha, J.E. Lim, M. Zhang, N. Bolan, D. Mohan, M. Vithanage, S.S. Lee, Y.S. Ok, Biochar as a sorbent for contaminant management in soil and water: A review, Chemosphere 99 (2014) 19–33.

[2] L. Dai, F. Tan, H. Li, N. Zhu, M. He, Q. Zhu, G. Hu, L. Wang, J. Zhao, Calcium-rich biochar from the pyrolysis of crab shell for phosphorus removal, J. Environ. Manag. 198 (2017) 70-74.
[3] A. Bello, N. Manyala, F. Barzegar, A.A. Khaleed, D.Y. Momodu, J.K. Dangbegnon, Renewable pine cone biomass derived carbon materials for supercapacitor application, RSC Adv. 6 (2016) 1800-1809.
[4] C. Jung, N. Phal, J. Oh, K.H. Chu, M. Jang, Y. Yoon, Removal of humic and tannic acids by adsorption–coagulationcombined systems with activated biochar, J. Hazard. Mater. 300 (2015) 808-814.
[5] G. Duman, Y. Onal, C. Okutucu, S. Onenc, J. Yanik, Production of activated carbon from pine cone and evaluation of its physical, chemical, and adsorption properties, Energy Fuels 23 (2009) 2197-2204.
[6] K.K. Shimabuk, J.P. Kearns, J.E. Martinez, R.B. Mahoney, L. Moreno-Vasquez, R.S. Summers, Biochar sorbents for sulfamethoxazole removal from surface water, stormwater, and wastewater effluent, Water Res. 96 (2016) 236-245.
[7] T. Sizmur, T. Fresno, G. Akgül, H. Frost, E. Moreno-Jiménez, Biochar modification to enhance sorption of inorganics from water, Bioresour. Technol. 246 (2017) 34-47.
[8] Y. Zhou, X. Liu, Y. Xianga, P. Wang, J. Zhanga, F. Zhanga, J. Wei, L. Luo, M. Lei, L. Tang, Modification of biochar derived from sawdust and its application in removal of tetracycline and copper from aqueous solution: Adsorption mechanism and modelling, Bioresour. Technol. 245 (2017) 266-273.
[9] D. Angın, E. Altintig, T.E. Köse, Influence of process parameters on the surface and chemical properties of activated carbon obtained from biochar by chemical activation, Bioresour. Technol. 148 (2013) 542-549.
[10] T.C. Chandra, M. MariaMirna, J. Sunarso, Y. Sudaryanto, S. Ismadjia, Activated carbon from durian shell: Preparation and characterization, J. Taiwan Inst. Chem. Eng. 40 (2009) 457–462.
[11] P. Liu, W.-J. Liu, H. Jiang, J.-J. Chen, W.-W. Li, H.-Q. Yu, Modification of bio-char derived from fast pyrolysis of biomass and its application in removal of tetracycline from aqueous solution, Bioresour.Technol. 121 (2012) 235-240.
[12] R. Li, J.J. Wang, B. Zhou, Z. Zhang, S. Liu, S. Lei, R. Xiao, Simultaneous capture removal of phosphate, ammonium and organic substances by MgO impregnated biochar and its potential use in swine wastewater treatment, J. Cleaner Prod. 147 (2017) 96-107.
[13] D. Xia, F. Tan, C. Zhang, X. Jiang, Z. Chen, H. Li, Y. Zheng, Q. Li, Y. Wang, $ZnCl_2$-activated biochar from biogas residue facilitates aqueous As(III) removal, Appl. Surf. Sci. 377 (2016) 361-369.
[14] L. Lonappan, T. Rouissi, R.K. Das, S.K. Brar, A.A. Ramirez, M. Verma, R.Y. Surampalli, J.R. Valero, Adsorption of methylene blue on biochar microparticles derived from different waste materials, Waste Manage. 49 (2016) 537-544.
[15] M. Taheran, M. Naghdi, S.K. Brar, E.J. Knystautas, M. Verma, A.A. Ramirez, R.Y. Surampalli, J.R. Valero, Adsorption study of environmentally relevant concentrations of chlortetracycline on pinewood biochar, Sci. Total Environ. 571 (2016) 772-777.
[16] A.U. Rajapaksha, S.S. Chen, D.C.W. Tsang, M. Zhang, M. Vithanage, S. Mandal, B. Gao, N.S. Bolan, Y.S. Ok, Engineered/designer biochar for contaminant removal/immobilization from soil and water: Potential and implication of biochar modification, Chemosphere 148 (2016) 276-291.
[17] S. Velten, D.R.U. Knappe, J. Traber, H.-P. Kaiser, U.v. Gunten, M. Boller, S. Meylan, Characterization of natural organic matter adsorption in granular activated carbon adsorbers, Water Res. 45 (2011) 3951-3959.
[18] E. Vuorio, R. Vahala, J. Rintala, R. Laukkanen, The evaluation of drinking water treatment performance with HPSEC, Environ. Int., 24(5/6) (1998) 617-623.
[19] A. Matilainen, N. Vieno, T. Tuhkanen, Efficiency of the activated carbon filtration in the natural organic matter removal, Environ. Int. 32 (2006) 324-331.
[20] M.R. Yazdani, N. Duimovich, A. Tiraferri, P. Laurell, M. Borghei, J.B. Zimmerman, R. Vahala, Adsorption and desorption of natural organic matter from lake water by tailored biochars, J. Mol. Liq. Data in Brief, Submitted (2019).
[21] S.A. Huber, A. Balz, M. Abert, W. Pronk, Characterisation of aquatic humic and non-humic matter with size-exclusion chromatography e organic carbon detection e organic nitrogen detection (LC-OCD-OND), Water Res. 45 (2011) 879-885.
[22] I. Langmuir, The constitution and fundamental properties of solids and liquids, J. Am. Chem. Soc. 38 (1916) 2221–2295.
[23] H.M.F. Freundlich, Over the adsorption in solution, Z. Physik. Chem. A57 (1906) 358-471.
[24] R. Sips, On the structure of a catalyst surface, J Chem. Phys. 16 (1948) 490-495.
[25] S. Lagergren, About the theory of so-called adsorption of soluble substances, Kungliga Svenska Vetenskapsakademiens Handlingar 24 (4) (1898) 1–39.
[26] Y.S. Ho, G. McKay, Pseudo-second order model for sorption processes, Process Biochem. 34 (5) (1999) 451–465.
[27] W.J. Weber, J.C. Morris, Kinetics of adsorption on carbon from solution, J. San. Eng. Div. Proc. Anal. Soc. Civil Eng. 89 (1963) 31-60.

[28] E. Apaydın-Varol, A.E. Pütün, Preparation and characterization of pyrolytic chars from different biomass samples, J. Anal. Appl. Pyrolysis 98 (2012) 29-36.
[29] F. Boudrahem, A. Soualah, F. Aissani-Benissad, Pb(II) and Cd(II) removal from aqueous solutions using activated carbon developed from coffee residue activated with phosphoric acid and zinc chloride, J. Chem. Eng. Data 56 (2011) 1946-1955.
[30] M.R. Yazdani, E. Virolainen, K. Conley, R. Vahala, Chitosan–Zinc(II) complexes as a bio-sorbent for the adsorptive abatement of phosphate: mechanism of complexation and assessment of adsorption performance, Polymers 10 (2018) 25.
[31] M. Yazdani, H. Bahrami, M. Arami, Feldspar/Titanium Dioxide/Chitosan as a biophotocatalyst hybrid for the removal of organic dyes from aquatic phases, J. Appl. Polym. Sci. 131 (2014) 40247.
[32] M.R. Yazdani, T. Tuutijärvi, A. Bhatnagar, R. Vahala, Adsorptive removal of arsenic(V) from aqueous phase by feldspars: Kinetics, mechanism, and thermodynamic aspects of adsorption, J. Mol. Liq. 214 (2016) 149-156.
[33] J. Liu, J. Cao, H. Chen, D. Zhou, Adsorptive removal of humic acid from aqueous solution by microand mesoporous covalent triazine-based framework, Colloids Surf. A 481 (2015) 276-282.
[34] B.M. Babic, S.K. Milonjic, M.J. Polovina, B.V. Kaludierovic, Point of zero charge and intrinsic equilibrium constants of activated carbon cloth, Carbon 37 (1999) 477-481.
[35] M.S. Rauthula, V.C. Srivastava, Studies on adsorption/desorption of nitrobenzene and humic acid onto/from activated carbon, Chem. Eng. J. 168 (2011) 35-43.
[36] H. Sehaqui, U.P.d. Larraya, P. Tingauta, T. Zimmermann, Humic acid adsorption onto cationic cellulose nanofibers for bioinspired removal of copper(II) and a positively charged dye, Soft Matter 11 (2015) 5294-5300.
[37] M.R. Yazdani, A. Bhatnagar, R. Vahala, Synthesis, characterization and exploitation of nano-TiO_2/feldsparembedded chitosan beads towards UV-assisted adsorptive abatement of aqueous arsenic (As), Chem. Eng. J. 316 (2017) 370-382.
[38] E. Worch, Adsorption Technology in Water Treatment : Fundamentals, Processes, and Modeling, DEU: Walter de Gruyter, Munchen, 2012.
[39] Q. Li, V.L. Snoeyinka, B.J. Marinasa, C. Campos, Pore blockage effect of NOM on atrazine adsorption kinetics of PAC: the roles of PAC pore size distribution and NOM molecular weight, Water Res. 37 (2003) 4863-4872.
[40] C. Pelekani, V. Snoeyink, Competitive adsorption in natural water: role of activated carbon pore size, Water Res. 33(5) (1999) 1209-1219.
[41] G. Hua, D.A. Reckhow, Characterization of disinfection byproduct precursors based on hydrophobicity and molecular size, Environ. Sci. Technol. 41(9) (2007) 3309-3315.
[42] L.J. Hem, H. Efraimsen, Assimilable organic carbon in molecular weight fractions of natural organic matter, Water Res. 35(4) (2001) 1106-1110.
[43] M. Teixidó, J.J. Pignatello, J.L. Beltrán, M. Granados, J. Peccia§, Speciation of the Ionizable Antibiotic Sulfamethazine on Black Carbon (Biochar), Environ. Sci. Technol. 45 (23) (2011) 10020–10027.
[44] W. Gwenzi, N. Chaukura, C. Noubactep, F.N.D. Mukome, Biochar-based water treatment systems as a potential low-cost and sustainable technology for clean water provision, J. Environ. Manage. 197 (2017).

Table content:

Table 1. Characteristics of the lake water.

Parameter	Raw	Treated with TB-N-I
pH	7.82	7.19
Conductivity [mS/cm]	0.206	0.224
Turbidity [FNU]	8.50	4.52
Color [mg/l Pt]	53.65	10.68
COD_{Mn}	13.4	4.38
NPOC	16.51	5.536
Total nitrogen [mg/l N]	4.2	1.49
Total phosphorus [µg/l P]	151	104

Table 2. BET analysis values.

Materials	BET surface area [m^2/g]	Pore volume [cm^3/g]	Pore size [nm]
Biomass	0.491	0.001	9.262
B-300	0.583	0.001	7.400
TB-N-I	1470.266	0.705	2.959
TB-Z-II	1067.902	0.511	2.681
PAC	819.475	0.325	4.291

Note: Adsorption cumulative isotherms were used to determine pore volume and pore size distribution via the Barret-Joyner-Halender (BJH) methodology.

Table 3. Engineered materials developed from forestry and agricultural wastes for pollutant removal.

Adsorptive material	Initial material	Surface area (m^2/g)	Pore volume (cm^3/g)	Pollutant	Sorption (mg/g)	Ref.
Acid/alkali-modified biochars	rice-husk	46.8, 117.8	0.033, 0.073	tetracycline	58.8	[11]
MgO-impregnated biochar	sugarcane crop residue	40.6-218.9	0.37-0.06	phosphate, ammonium humate	398 22 247	[12]
$ZnCl_2$- activated biochar	biogas residue	516.67	0.24	arsenite	27.67	[13]
Biochar	wood and sludge	400	-	sulfamethoxazole antibiotic	-	[6]
Biochar microparticles	pig manure	-	-	methylene blue	25	[14]
Activated Biochar	pinewood	852.95	-	chlortetracycline	208.3	[15]
Tailored mesoporous biochar	pinecone	1470	0.705	NOM	36	this work

Table 4. Calculated kinetic parameters for the adsorption of NOM.

Material	$q_{e(exp)}$	Pseudo-first-order				Pseudo-second-order				Intraparticle diffusion	
		$q_{e(cal)}$	k_1	r^2	Δq	$q_{e(cal)}$	k_2	r^2	Δq	k_{ip}	C
		Nonlinear								Linear	
TB-N-I	38.15	33.16	0.629	0.667	0.161	34.85	0.023	0.814	0.124	0.411	25.65
TB-N-II	18.16	14.13	0.817	0.588	0.182	14.71	0.080	0.655	0.153	0.183	11.04
TB-Z-II	14.45	11.76	0.092	0.655	1.333	12.24	0.013	0.753	0.684	0.253	6.06

Table 5. Adsorption isotherm parameters for the adsorption of NOM calculated via nonlinear regression.

Model	Material	Parameter				
Langmuir		q_L (mg/g)	K_L (L/mg)	r^2	Δq	
	TB-N-I	180.24	0.064	0.953	0.373	
	PAC	133.24	0.072	0.967	0.184	
Freundlich		K_F (mg/g)/(mg/L)$^{1/n}$	1/n	r^2	Δq	
	TB-N-I	9.446	0.985	0.984	0.081	
	PAC	9.763	0.795	0.965	0.189	
Sips		q_S (mg/g)	K_S (L/mg)^{ns}	n_S	r^2	Δq
	TB-N-I	143.97	0.058	1.330	0.988	0.080
	PAC	127.99	0.075	1.012	0.967	0.103

Table 6. Average results and standard deviation of LC-OCD analysis for raw lake water and PAC and TB-N-I effluents. MM denotes molar mass.

Sample	Chromato-graphic DOC (µg/l)	Bio-polymers (µg/l)	Humic Substances (HS) (µg/l)	MM of HS (g/mol)	Building Blocks (µg/l)	Low MM Neutrals (µg/l)	Low MM Acids (µg/l)
Raw water	10169	246	6921	534	1495	1450	57
PAC	4148 ± 19.3	187 ± 3.0	2784 ± 31.3	572 ± 13	465 ± 19.9	605 ± 12.3	106 ±15.3
TB-N-I	2732 ± 69.9	96 ± 0.8	1813 ± 53.5	656 ± 42.0	388 ± 74.4	324 ± 36.4	111 ± 13.3

Figure content:

Figure 1. FTIR spectra (a) and TGA thermograms (b) of the tailored and initial materials. Nitrogen adsorption-desorption isotherms (c), pore size distribution (d), and SEM images of TB-N-I (e).

Figure 2. NOM (a) and color (b) removal from lake water by varying adsorbent dosage after 24 h contact time. (c) NOM removal at different dilutions by 0.25 g/L TB-N-I at 0.5, 30, and 1440 min contact times - Experimental condition: room temperature; natural pH.

Figure 3. Effect of pH on NOM (a) and color (b) removals from lake water by the tailored and initial materials - Experimental condition: optimized adsorbent dosage; 24 h contact time; room temperature.

Figure 4. Effect of contact time on NOM (a) and color (b) removals from lake water by the tailored and initial materials - Experimental condition: optimized adsorbent dosage; natural pH; room temperature.

Figure 5. a) Intra-particle diffusion plots for NOM adsorption onto tailored biochars. b) Equilibrium experimental (markers) and theoretical data (lines) plotted via non-linear regression for NOM adsorption onto TB-N-I and PAC.

Figure 6. LC-OCD chromatograms obtained with organic carbon detection (a) and UV detection (b) for influent and effluent samples of PAC and TB-N-I.

Figure 7. Schematic illustration of key mechanisms involved in NOM adsorption from lake water by tailored mesoporous biochars.

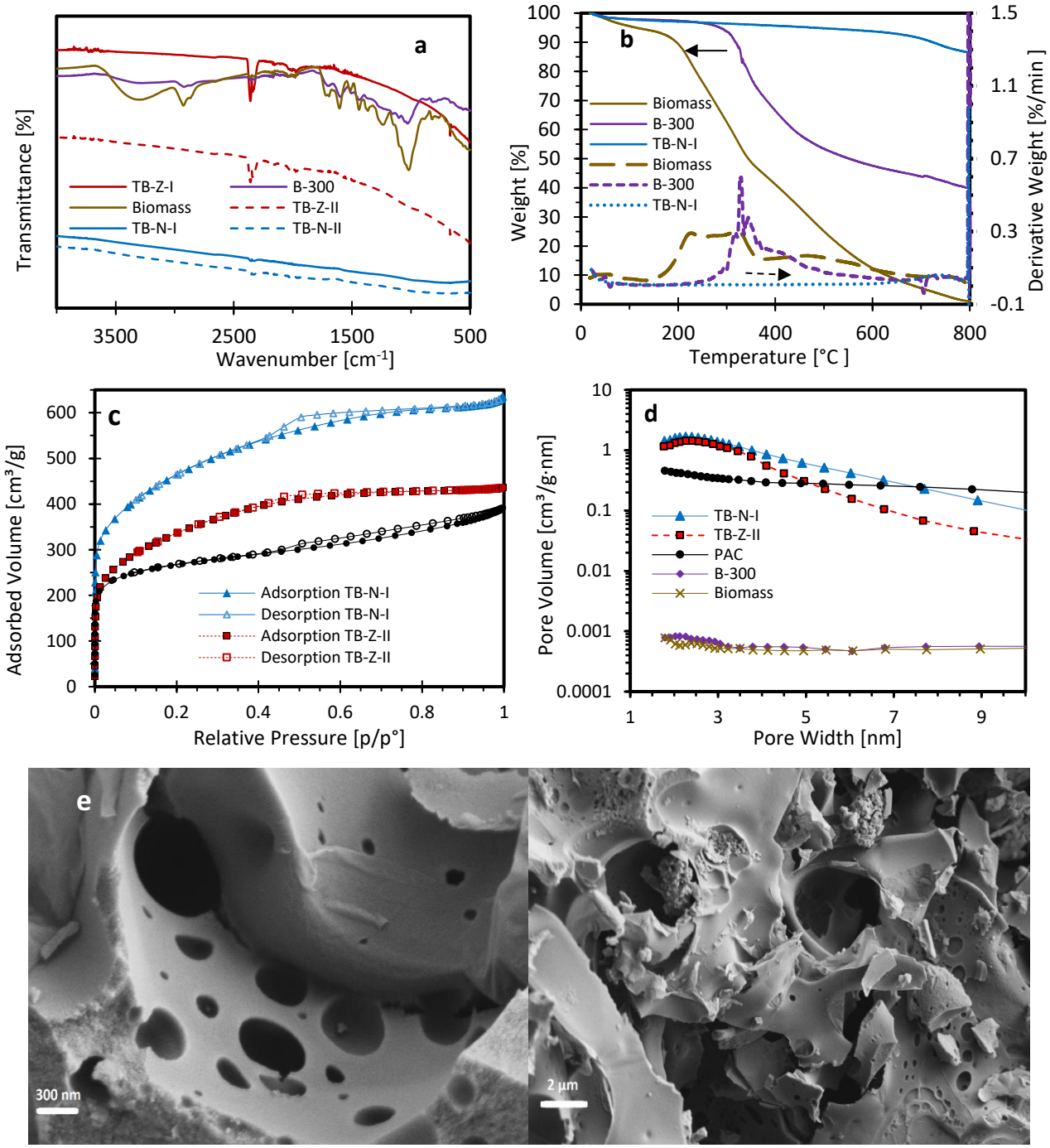

Figure 1. FTIR spectra (a) and TGA thermograms (b) of the tailored and initial materials. Nitrogen adsorption-desorption isotherms (c), pore size distribution (d), and SEM images of TB-N-I (e).

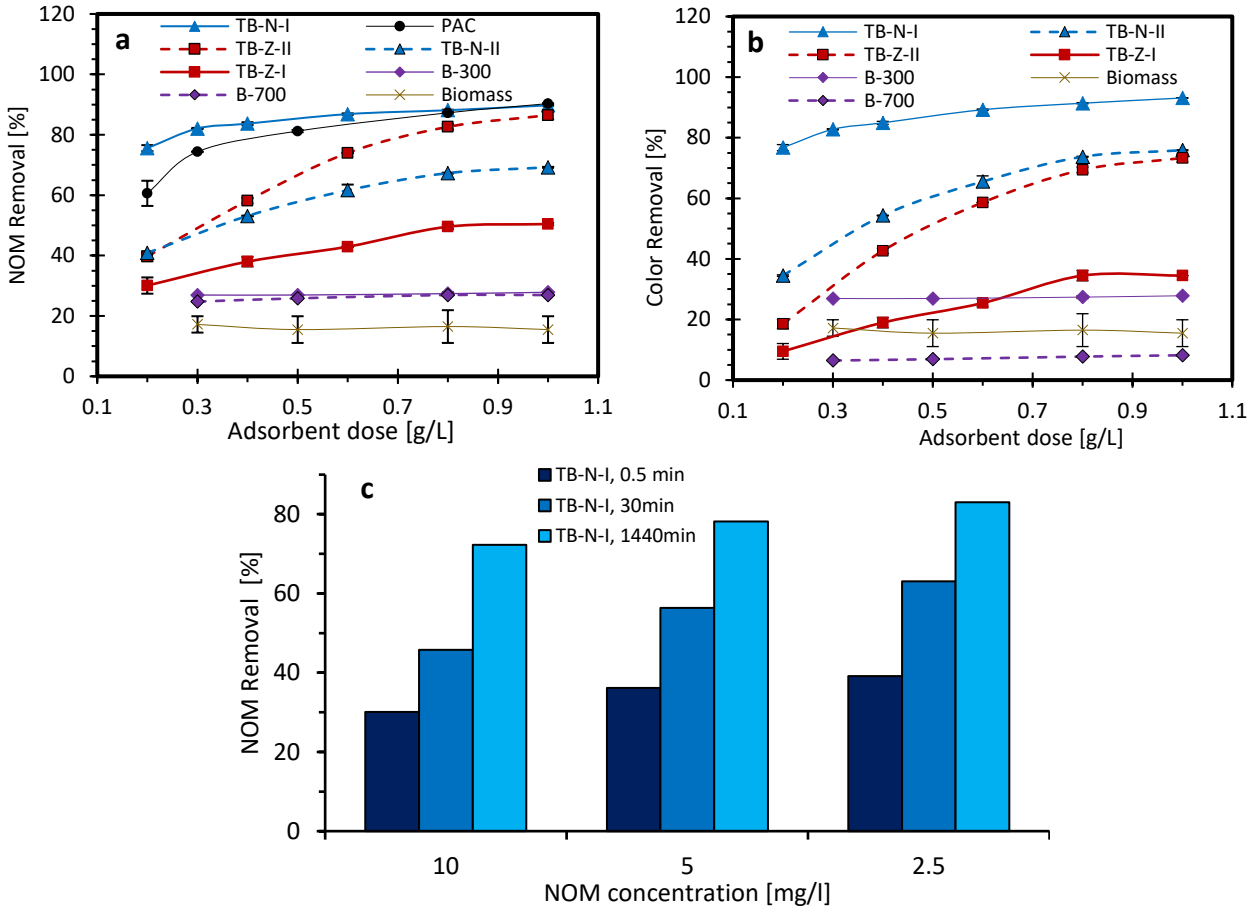

Figure 2. NOM (a) and color (b) removal from lake water by varying adsorbent dosage after 24 h contact time. (c) NOM removal at different dilutions by 0.25 g/L TB-N-I at 0.5, 30, and 1440 min contact times - Experimental condition: room temperature; natural pH.

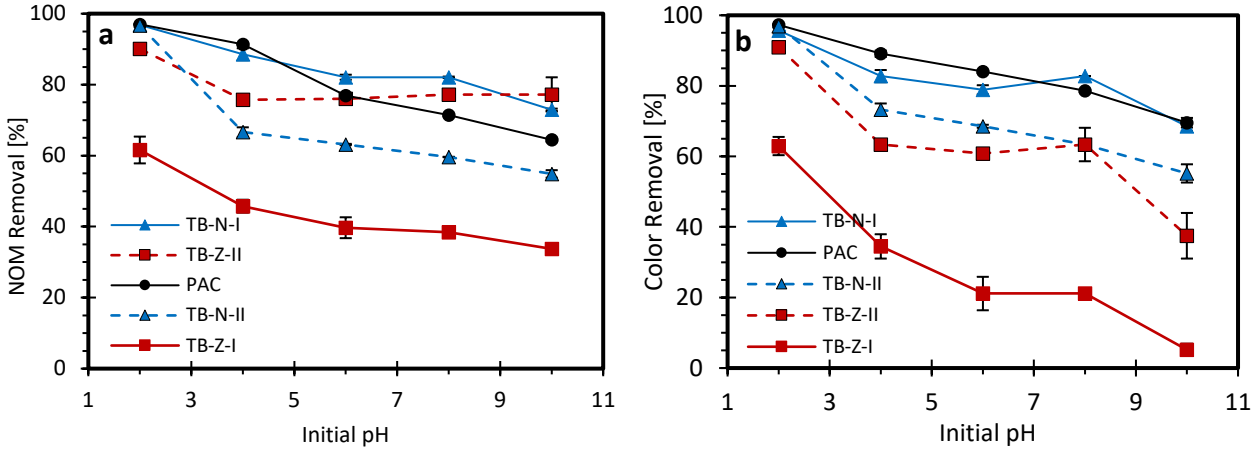

Figure 3. Effect of pH on NOM (a) and color (b) removals from lake water by the tailored and initial materials - Experimental condition: optimized adsorbent dosage; 24 h contact time; room temperature.

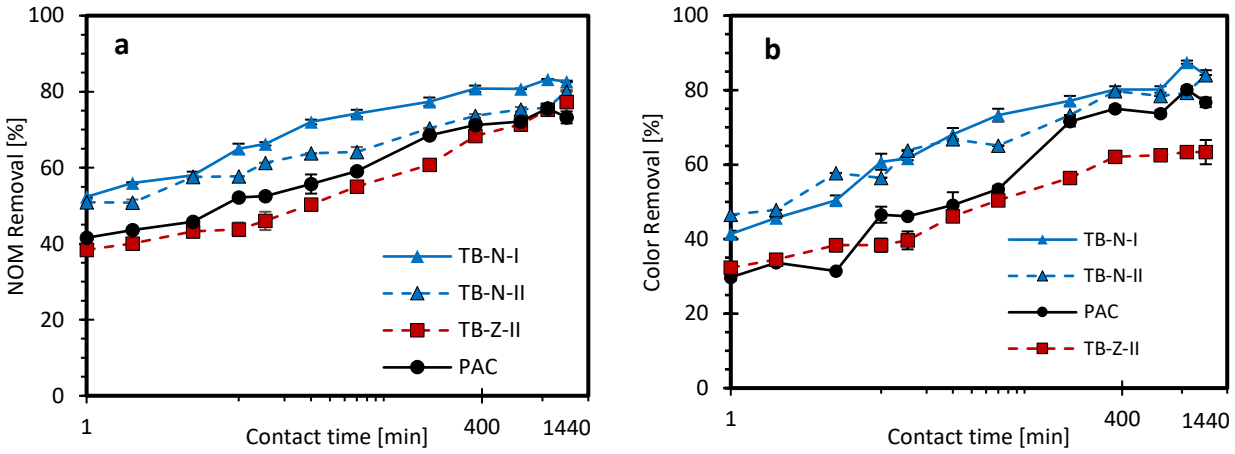

Figure 4. Effect of contact time on NOM (a) and color (b) removals from lake water by the tailored and initial materials - Experimental condition: optimized adsorbent dosage; natural pH; room temperature.

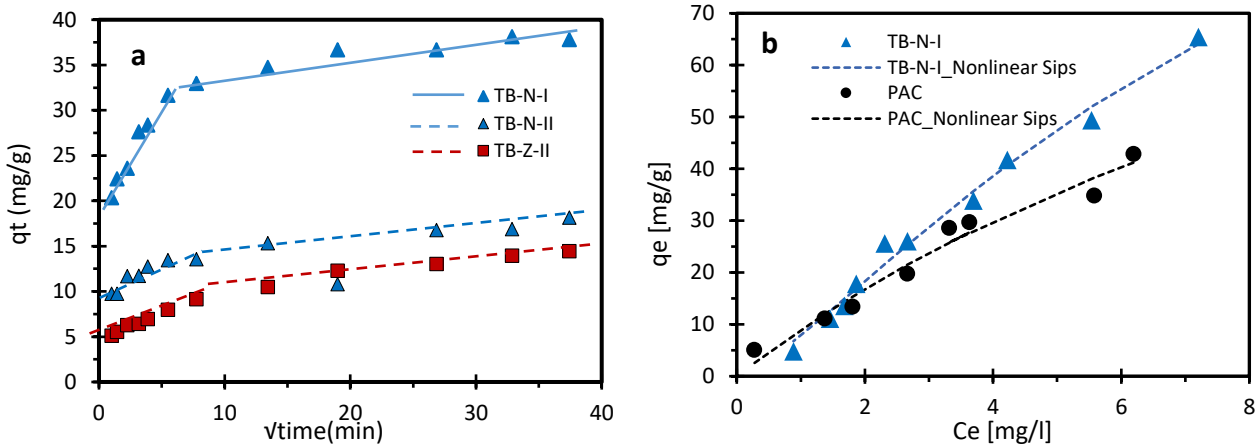

Figure 5. a) Intra-particle diffusion plots for NOM adsorption onto tailored biochars. b) Equilibrium experimental (markers) and theoretical data (lines) plotted via non-linear regression for NOM adsorption onto TB-N-I and PAC.

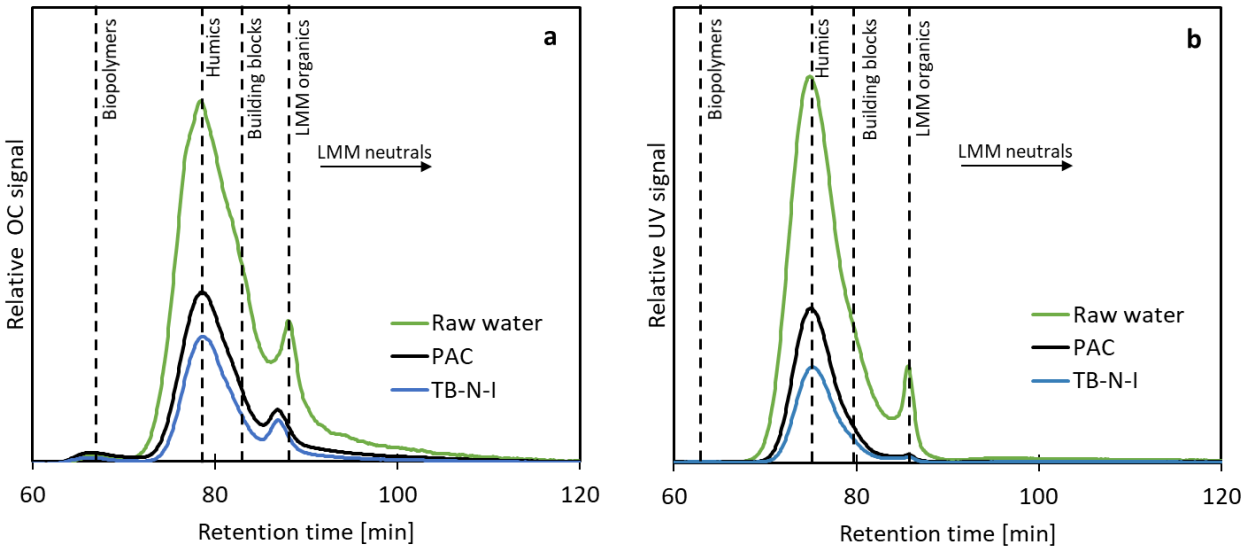

Figure 6. LC-OCD chromatograms obtained with organic carbon detection (a) and UV detection (b) for influent and effluent samples of PAC and TB-N-I.

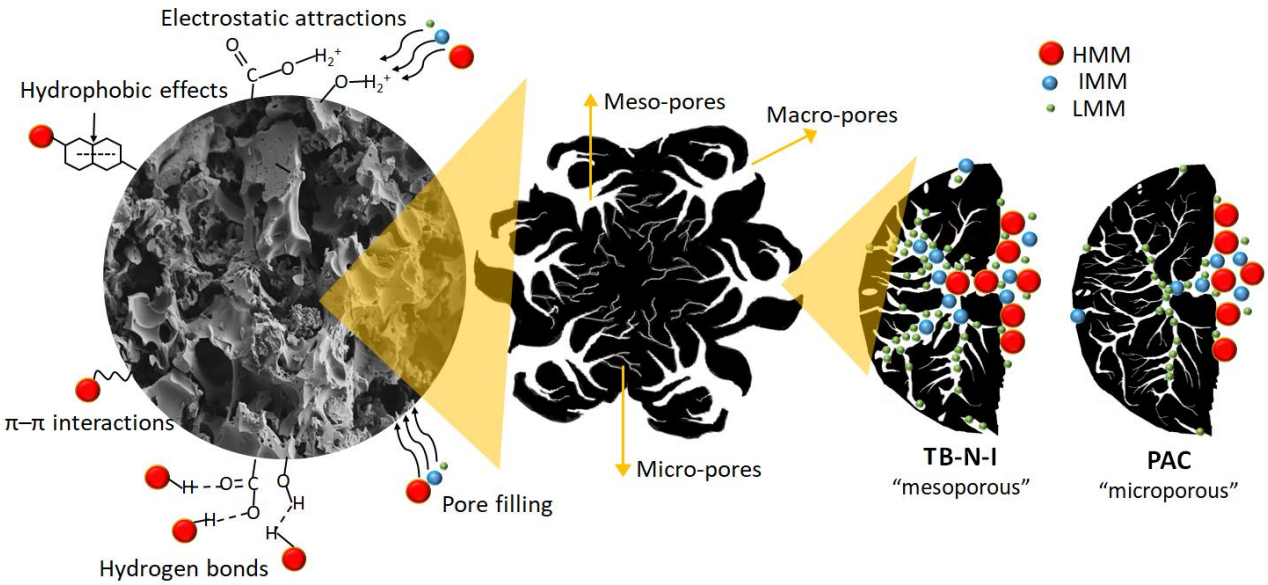

Figure 7. Schematic illustration of key mechanisms involved in NOM adsorption from lake water by tailored mesoporous biochars.